www.czasopisma.pan.pl PAN www.journals.pan.pl
Opto-Electronics Review 27 (2019) 143–148

Contents lists available at ScienceDirect

Opto-Electronics Review

journal homepage: http://www.journals.elsevier.com/opto-electronics review

Electrical and optical properties of nanowires based solar cell with radial p-n junction

O.V. Pylypova [b], A.A. Evtukh [a,b], P.V. Parfenyuk [a], I.I. Ivanov [b], I.M. Korobchuk [b], O.O. Havryliuk [c,*], O.Yu. Semchuk [c]

[a] *V. Lashkaryov Institute of Semiconductor Physics NAS of Ukraine, 41 pr. Nauki, Kyiv 03028, Ukraine*
[b] *Taras Shevchenko National University of Kyiv, 60 Volodymyrska St., Kyiv 01033, Ukraine*
[c] *Chuiko Institute of Surface Chemistry NAS of Ukraine, 17 Ganeral Naumova St., Kyiv 03164, Ukraine*

ARTICLE INFO

Article history:
Received 4 March 2019
Received in revised form 29 April 2019
Accepted 14 May 2019
Available online 31 May 2019

Keywords:
Nanowire array
Solar cell
Light trapping
Reflectance
Metal assisted chemical etching

ABSTRACT

In our studies the absorption, transmittance and reflectance spectra for periodic nanostructures with different parameters were calculated by the FDTD (Finite-Difference Time-Domain) method. It is shown that the proportion of reflected light in periodic structures is smaller than in case of thin films. The experimental results showed the light reflectance in the spectral range of 400–900 nm lower than 1% and it was significantly lower in comparison with surface texturing by pyramids or porous silicon.

Silicon nanowires on p-type Si substrate were formed by the Metal-Assisted Chemical Etching method (MacEtch). At solar cells with radial p-n junction formation the thermal diffusion of phosphorus has been used at 790 °C. Such low temperature ensures the formation of an ultra-shallow p-n junction. Investigation of the photoelectrical properties of solar cells was carried out under light illumination with an intensity of 100 mW/cm^2. The obtained parameters of NWs' solar cell were I_{sc} = 22 mA/cm^2, U_{oc} = 0.62 V, FF = 0.51 for an overall efficiency η = 7%. The relatively low efficiency of obtained SiNWs solar cells is attributed to the excessive surface recombination at high surface areas of SiNWs and high series resistance.

© 2019 Association of Polish Electrical Engineers (SEP). Published by Elsevier B.V. All rights reserved.

1. Introduction

In recent decades, many studies aimed at developing new designs of solar cells, in order to reduce the cost of their production and increase the productivity of their work. A number of approaches have been proposed that can significantly improve performance and reduce the cost of photovoltaic (PV). Interesting researches are the PV structures based on nanostructured materials such as nanotubes, nanorods, nanopillars, nanowires that promote better light absorption and efficient charge separation due to their large surface areas. Semiconductor nanowires are promising candidates for the creation of photovoltaic devices on their basis [1–3].

Compared to bulk silicon, the silicon nanowires' (Si NWs) array shows unique electrical and optical properties, making its the potential candidate for photovoltaic applications [4,5]. Si NWs allow to reduce the optical losses, increase the optical absorption, and improve the carrier extraction for high-performance and low-cost solar cells [6–8]. The radial (coaxial) p-n-junction can provide an efficient carrier collection, and an open array structure can significantly improve optical absorption. Solving the issue of efficient light capture is very important, especially if the thickness of the silicon substrate is reduced [9–11]. Fine surface structures containing elements on a nanometer scale can provide excellent characteristics for light trapping (anti-reflection) performance [12,13].

The absorption of light can be attributed to three main mechanisms. First, the silicon nanowires array structure has an extremely small reflection coefficient due to the large open area on the front surface. Secondly, each individual nanowire is a nanosized cylindrical resonator that can trap light by repeated internal reflection. Third, the strong diffusion of light between nanowires causes further delight in light, since the diameter and period of arrays of nanowires usually have an order proportional to the optical wavelength. These mechanisms are quite sensitive to the structural parameters of nanowires array.

The growth of Si nanowires (Si-NWs) is especially promising. A recently developed metal-assisted chemical etching (MacEtch) method is simple and cheap process to produce Si NWs [13,14].

The purpose of this work is theoretical and experimental studies of light trapping by Si-NWs on the silicon surface depending on

* Corresponding author.
E-mail addresses: anatoliy.evtukh@gmail.com (A.A. Evtukh), gavrylyuk.oleksandr@gmail.com (O.O. Havryliuk).

https://doi.org/10.1016/j.opelre.2019.05.003
1230-3402/© 2019 Association of Polish Electrical Engineers (SEP). Published by Elsevier B.V. All rights reserved.

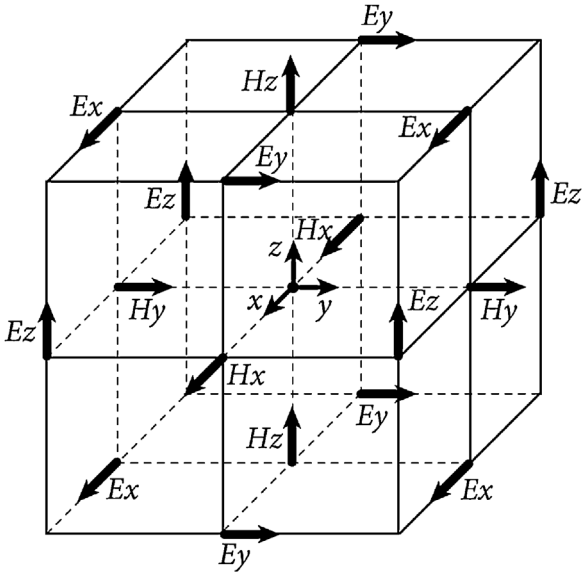

Fig. 1. Yee grid pattern.

their parameters and investigations of the properties of nanowires' based solar cell with radial p-n junction.

2. Theory

There are many methods of numerical electrodynamics. But the most widely used method of electromagnetic modeling is the Finite-Difference Time-Domain method (FDTD). The FDTD method is a powerful numerical algorithm for direct solution of Maxwell's equations. The advantage of this method is the simplicity and the ability to obtain results for a wide range of wavelengths in one calculation, as well as the ability to specify properties of materials at any point of the calculation grid, which allows considering anisotropic, dispersed and nonlinear media. This method can be precisely applied to general electromagnetic structures, including free-form particles [15]. At the same time, the FDTD method can be very resource-consuming, especially when simulating long objects. This method requires 10–30 dots per wavelength, while small wavelengths determine a very thick sampling rate. This leads to cumbersome calculations, especially in three dimensions. Therefore, in our calculations, we use two dimensions.

The realization of this method is discrete both in space and in time. The time step is chosen to provide numeric stability and is related to the size of the grid [16]. The presented structures are described on a discrete mesh consisting of Yee cells (Fig. 1), and the Maxwell equation is solved discretely over time on this grid. The grids of the electric and magnetic fields are shifted relative to each other by half the sampling step for each of the spatial variables and by time. As a result, the nodes corresponding to components E are arranged in such a way that each of them is surrounded by four components of H, and vice versa. To calculate the values of E in the time step $n + 1/2$, the value of H is used in step n. Similarly, the values of H in step $n + 1$ are calculated using the values of E in step $n + 1/2$. So, consistently values of all fields are calculated. Thus, finite-difference equations allow us to determine the electric and magnetic fields at a given time step based on the known field values on the previous one, and under given initial conditions the computational procedure gives a solution in time from the beginning of the reference with a given time step.

There are a lot of scalable grids, but we will use the most widespread Yee grid. The location of nodes in such a grid is shown in Fig. 1.

For calculations of optical spectra, the following Maxwell equations [17] are used:

$$\frac{\partial \vec{E}}{\partial t} = \frac{1}{\varepsilon}\left(\nabla \times \vec{H}\right) \tag{1}$$

$$\frac{\partial \vec{H}}{\partial t} = -\frac{1}{\mu}\left(\nabla \times \vec{E}\right), \tag{2}$$

where E and H are the electric and magnetic fields, respectively, μ is the permeability, ε is the dielectric permittivity of the medium.

Any change in the field E in time is to be associated with a change in the field H through space, and vice versa, which is the basis for using the FDTD method. Using the Fourier transform, one can obtain a frequency solution and calculate the transmission, reflection and absorption spectra.

To eliminate the nonphysical rebound of an electromagnetic wave from the boundary of the computational domain and to simulate the output of the wave to infinity, special absorbing boundary conditions should be used in the FDTD method. Currently, the most successful implementation of these conditions is the placement of a thin layer of special material along the boundary of the computing area, the so-called perfectly matched layer (Perfectly Matched Layer – PML). This material practically completely absorbs all the incident waves without any reflection regardless of the angle of incidence and the wavelength. PML is just an area that has anisotropic and complex-significant dielectric and magnetic permeability. Although the PML layers are purely theoretical and non-reflective, however, they exhibit some reflective properties due to errors in the numerical sampling of the problem: grids' partition. To minimize this reflection, you need to apply a PML split that takes into account the anisotropy of the properties of the material. PML can be interpreted mathematically as stretching or compression of coordinates using complex-valued functions based on the analytic continuation of Maxwell's equations in a complex plane in such a way that their solution exponentially decays [18].

Bloch type boundary conditions are applied to the vertical districts of the calculated region. Bloch type boundary conditions are very similar to periodic boundary conditions, which copy the fields at one boundary of the simulation area and reuse them at another boundary. But Bloch's boundary conditions use phase correction during copying of such fields, which enables more precise modeling of the task.

According to Bloch theorem, for periodic structure field components have the following properties:

$$\vec{\Psi}\left(\vec{r} + \vec{R}, t\right) = \Psi\left(\vec{r}, t\right) e^{i \to kr}, \tag{3}$$

where $\to R$ is the lattice vector, $\to k$ is the wave vector.

For our case, the field inside the periodic structure adopts the same symmetry and frequency as the structure itself:

$$\to E\left(\vec{r}\right) = \vec{A}\left(\vec{r}\right) e^{i\vec{\beta}\vec{r}}, \tag{4}$$

where $\to E\left(\vec{r}\right)$ is the overall field, $\to A\left(\vec{r}\right)$ is the amplitude envelope with same periodicity and symmetry as the device, $e^{i\vec{\beta}\vec{r}}$ is the phase shift.

For a structure having periodicity in coordinate x with period P_x, the Bloch theorem can be rewritten as follows:

$$\vec{E}\left(x \pm P_x\right) = \vec{E}\left(x\right) e^{\pm i\beta_x P_x}. \tag{5}$$

As a source of radiation, a plane wave is used. In our theoretical investigation, we use the solar spectrum AM1.5. The sources of plane waves are used to supply transverse-homogeneous electromagnetic energy from one side of the source region. In case of two-dimensional simulation, the source of plane waves is set along the line. In our calculations the range of wavelengths of

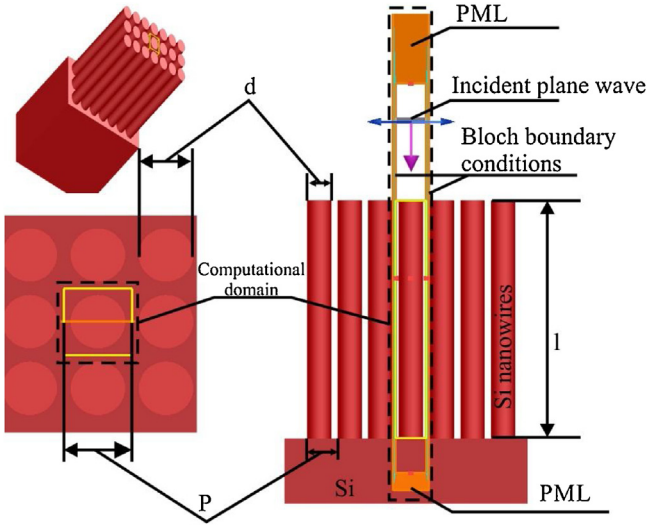

Fig. 2. Cross section of the simulation model.

300–1240 nm is used. The scheme used for theoretical calculations is shown in Fig. 2.

In the simulation the following parameters of the investigated structure are used: $d/P = 0.8$ ($d/P = 0.8$–0.9 the optimal ratio for better absorption of solar energy [19–21]), $l = 2330$ nm, d between 50–240 nm. (d is the diameter of nanowires, P is the period, l – length of nanowires) (Fig. 2). A comparison was made between semiconductor structures with nanowires of different diameters and length.

3. Experimental

P-type (100) one-sided polished silicon substrates with specific resistance of 10 Ω × cm were used for silicon nanowires (Si NWs) array fabrication. Silicon nanowires' array was formed by metal assisted chemical etching (MacEtch) method. The Si NWs formation by MacEtch included two stage processes. At the first stage the Ag nanoparticles were deposited on the silicon surface from $AgNO_3$/HF solution. In our experiments the silver particles were deposited in the solution of 0.02 M $AgNO_3$/4.6 M HF for 2 min. At the second stage the silicon is etched in HF / H_2O_2 solution under the Ag particles. The existence of the metal particles on the Si surface enhances the velocity of Si etching in HF/H_2O_2 solution. In our case the silicon wafers were etched in the solution of 0.15 M H_2O_2/4.6 M HF for 30 min. The detailed description of the electrochemical processes during formation of Si NWs by MacEtch is presented elsewhere [13,22–24].

The morphology of the etched samples and the nanowires' size was determined using high resolution scanning electron microscopy (HR SEM: model LEO440UP, Hitachi S - 4800). Experimental measurement of reflection was performed using a spectrophotometer (Shimadzu, model UU3101PC).

To determine the advantages of Si-NWs based solar cells (SCs) design, the SC with radial (coaxial) p-n junction have been prepared (Fig. 3). The advantages of such SCs are: (i) short travel distances of photoexcited minority carriers to the collection electrodes leading to enhanced carrier-collection efficiency and minimum bulk recombination; (ii) high tolerance of PVs for material defects permitting the use of lower quality Si with shorter minority-carrier diffusion lengths [25].

Technological processes for preparation of Si NWs based SC with radial p-n junction are described in detail in our previous article [22]. Among main processes of technological route are (*i*) deposition of silver nanoparticles to the surface of the silicon substrate; (*ii*) formation of Si nanowires by MacEtch; (*iii*) creation of radial p-n-junctions on the surface of Si NWs by thermal diffusion from liquid phosphorus source; (*iv*) creation of the back contact by sputtering of Al film and subsequent annealing at the temperature of 380 °C; (*v*) creation of a current-collecting upper contact that adjoins the n-region of radial p-n-junction by deposition of Al film (see Fig. 3).

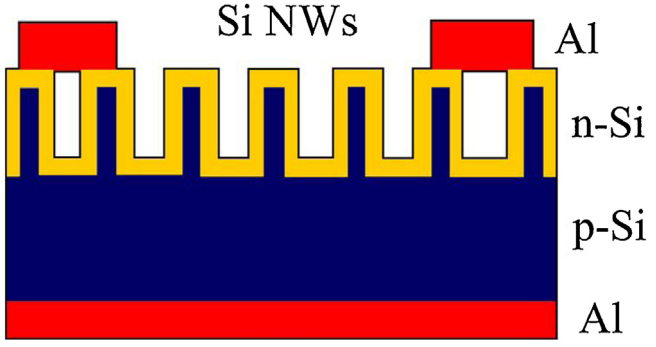

Fig. 3. Schematic image of NWs SC with radial p-n junction.

The measurements of dark and under illumination current-voltage (I–V) characteristics of solar cell were performed by an automated complex consisting of a universal device Keithley Source Meter Series 2410. Its feature is that it automatically controls the voltage source between the upper and bottom contacts of metal-insulator-semiconductor structures at the same time measures the current. The data transmission was carried out through the GPIB-USB device to the PC. As a program for automatically measuring and collecting the data we used the LabTracer 2.0 software package from Keithley Instruments. The solar simulator based on halogen lamps with light intensity 100 mW/cm^2 has been used.

4. Results and discussion

The obtained value of the reflection coefficient for silicon is of about 30 percent and it begins to increase with the approach to the direct interband transition (3.4 eV), with corresponding peaks of 280 and 370 nm [Fig. 4*a*)]. These peaks are also stored in the reflection spectra of structures with other diameters of nanowires [Peaks 1 and 2 in Fig. 4*b*)].

At energies below the border of the forbidden band (wavelength (λ) > 1100 nm) absorption coefficient value $\alpha < 1$ cm^{-1} and all the light is absorbed in the silicon layer thickness $L > 1$ cm. As well as the thickness of the silicon wafer is of about 300–500 microns, this layer can be considered transparent to light with $\lambda > 1100$ nm. As the wavelength decreases, value α begins to increase and the light is absorbed in a layer of smaller thickness. For example, a light with $\lambda = 1000$ nm is absorbed in a layer of c-Si thickness of 100 μm, and light with $\lambda = 400$ nm is absorbed in a layer of c-Si thickness of 10 nm. Therefore, the region $\lambda < 1100$ nm is a strong absorption region [26].

The intensity of the scattered light at right incidence angle strongly depends on the wavelength λ of the incident radiation, as well as on the diameter of the structures investigated. For a light with $\lambda < 370$ nm, only an increase in the scattering intensity peaks is observed with increase in the diameter of the nanowires (Fig. 4), which may be due to high values of the imaginary part of the refractive index at energies greater than the energy of a direct interband transition in c-Si at 370 nm (3.4 eV). For $\lambda > 400$ nm, the scattering intensity shows a branched structure. At diameters of nanowires of 50–90 nm, the appearance of new peaks (peaks 3) is observed in the range of 400–500 nm wavelengths which are not observed on the reflection spectra of the c-Si film [Fig. 4*a*)]. With a further increase of the nanowires' diameter a shift is observed of these

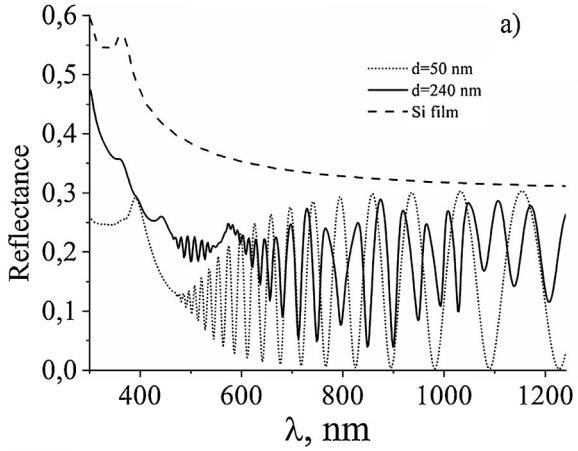

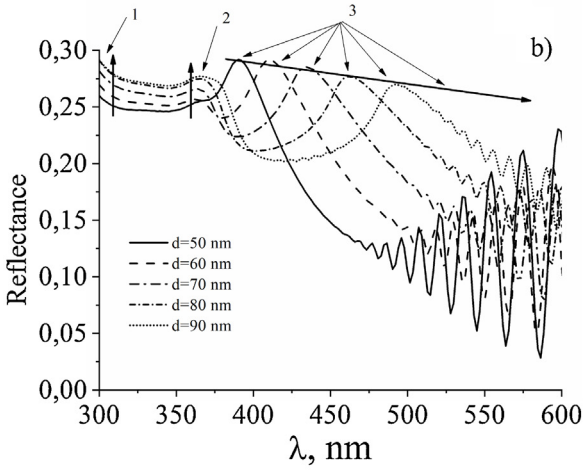

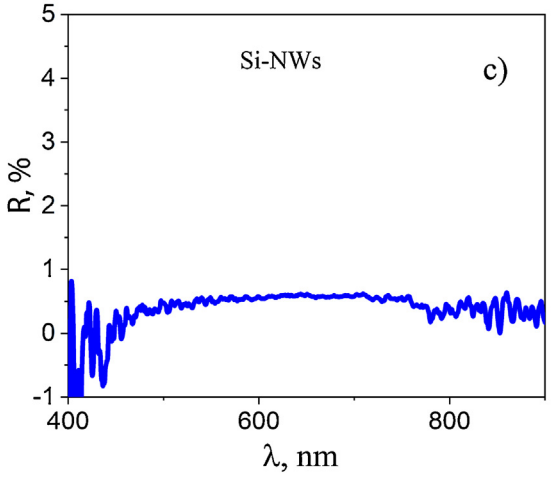

Fig. 4. Reflectance spectra of the structures with nanowires of various diameters: *a*) $d = 50$ nm, $d = 240$ nm, the dash line shows the reflection spectrum of the silicon wafer, *b*) $d = 50, 60, 70, 80, 90$ nm, *c*) Spectra of optical reflection of the light from the real silicon surface with Si-NWs (after smoozing).

peaks to the long-wave region, while at their place in the region of 400–450 nm peaks of intensity of light dispersion appear again. It should be noted, however, that the intensity of reflection of structures with nanowires is much less than that of crystalline silicon over the entire range of calculated wavelengths [Fig. 4*a*)], due to a decrease in the density of the structure with nanowires, which also causes an increase in the transmittance (Fig. 5). The high area of

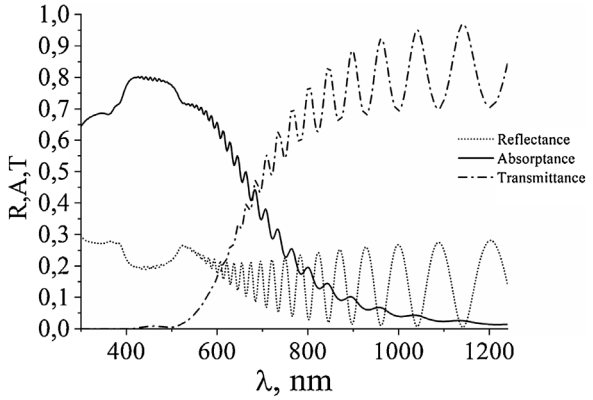

Fig. 5. Reflection, absorption and transmission spectra for a structure with nanowires with a diameter of 100 nm.

silicon nanowires leads to multiple scattering of sunlight between nanowires, which also increases the absorption coefficient (Fig. 5).

In the region of low energies, the length of the light wave is much longer than periodicity of nanowires in nanostructures, so the radiation can easily penetrate through the silicon nanostructure and interact with the silicon substrate. In the region of high energies, when the wavelength becomes close to the period of nanostructures, absorption of light will be enhanced due to the strong scattering effect (Fig. 5), which increases the length of the optical path [19,27–29]. The higher transmittance of nanowires is not compensated by the low reflection coefficient, which leads to insufficient absorption of low-energy photons. Conversely, virtually zero transmittance in the high-energy region and a low reflection coefficient contribute to increase in the absorption coefficient of high-energy photons.

At wavelengths greater than 500 nm, reflection spectra show Fabry-Perot resonances. The appearance of such interference effects in the spectra is due to the repeated reflection of radiation from the boundaries of nanostructures. In the case of thermal reflection this phenomenon may be due to the modulation of the refractive index in the area of a spatial charge or with its thermal dependence [30].

At shorter wavelengths, we can see a decrease in resonances. This can be explained by an increase in absorption by bulk silicon, which suppresses resonances, but ensures that all light coming into the array will be absorbed in one pass [31]. Interference effects can also be explained by an increase in the field concentration inside the nanowires and the excitation of wave resonance modes.

The SEM images of obtained Si NWs are presented in Fig. 6. The diameters of the nanowires are in the range of 60–160 nm and the lengths are of 2100–2300 nm.

The analysis of optical reflection of the light from the silicon surface with the formed nanowires points out on high light trapping. The reflection coefficient in a wide range of wavelengths (400–900 nm) was less than 1% [Fig. 4*c*)].

The current-voltage characteristics of the prepared Si NWs' solar cell with the size of 2×3 cm^2 under illumination with intensity of 100 mW/cm^2 are presented in Fig. 7. Main parameters of SC determined from I–V characteristics are: short circuit current density J_{sc} = 22 mA/cm^2, open circuit voltage V_{oc} = 0.62 V, fill factor $FF = 0.51$, and conversion efficiency $\eta = 7\%$. The obtained parameters are averaged and the range of efficiency variation was from 5 to 11%. The further improvement will be after Si NWs' surface passivation and optimization of p-n junction formation conditions. The relatively low efficiency of obtained SiNWs' solar cells is attributed to the excessive surface recombination at high surface areas of SiNWs and high series resistance.

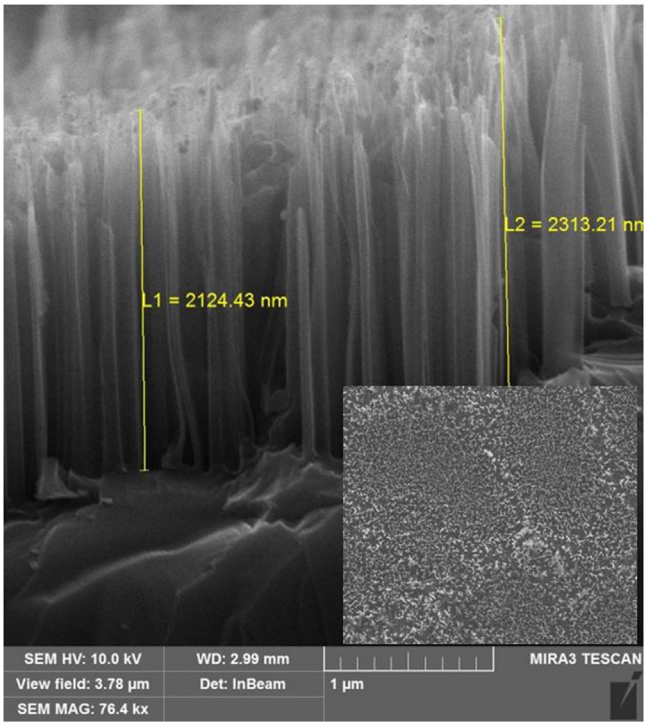

Fig. 6. SEM image of obtained cross section view of Si NWs. In insert: top view of Si NWs.

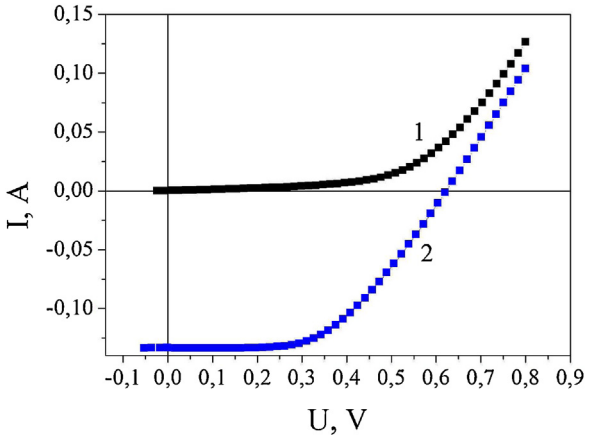

Fig. 7. I–V characteristics of Si NWs SC in dark (1) and under illumination with intensity of 1 KW/m^2 (2).

To estimate the influence of shunt and series resistance the dark I–V characteristics has been rebuilt in semi-logarithmic scale (Fig. 8). Ideality coefficient (n) is significantly higher value of $n = 1$ for some parts of curve. It points out on existence low shunt and large series resistances.

As can be seen, the further improvement of Si NWs SC parameters is connected with the reduction of the influence of the shunt and series resistances. The series resistance of Si NW has to be decreased.

It is very important to determine which part of Si NW p-type core or n-type doping layer restricts the current flow. For this, the doping n-type impurity distribution and depth of p-n junction in Si NW for our diffusion conditions have been calculated based on Fick's diffusion equation [32]:

$$\frac{\partial C}{\partial t} = D\frac{\partial^2 C}{\partial^2 x^2}, \tag{6}$$

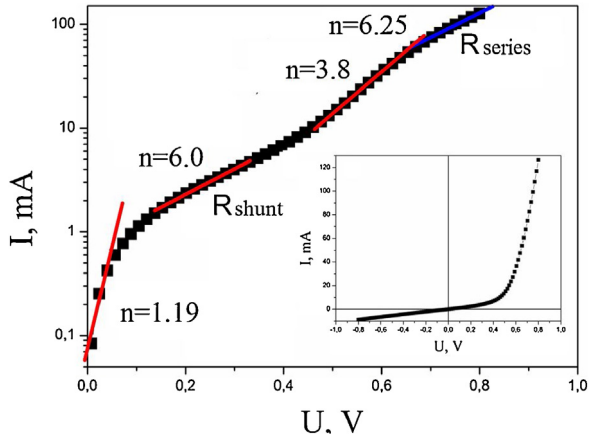

Fig. 8. Dark I–V characteristics of Si NWs SC in semi-logarithmic scale. In insert: the same in linear scale.

where C is the impurity concentration, x is the depth of diffusion, t is the time of diffusion, D is the diffusion coefficient of the impurities (phosphorous in our case) in the silicon.

To build a distribution profile of impurities in the case of two-stage diffusion it is necessary to know the temperature and duration of the first and second stages. The temperature of the first stage process T_1 specifies the diffusion coefficient of impurities at this stage D_1 and the surface concentration C_{01} which is determined by the limiting solubility of the impurities.

After the solution of Eq. (6), the distribution of the impurities after the second stage can be defined using the following expressions:

$$C(x,t) = \frac{2C_{01}}{\pi}\sqrt{\frac{D_1 t_1}{D_2 t_2}}\exp\left(-\frac{x^2}{4D_2 t_2}\right) = \frac{N}{\sqrt{\pi D_2 t_2}}\exp\left(-\frac{x^2}{4D_2 t_2}\right), \tag{7}$$

$$N = \int_0^\infty C(x)\,dx = \int_0^\infty C_{01}\,\mathrm{erfc}\frac{x}{2\sqrt{D_1 t_1}}dx = 2C_{01}\sqrt{\frac{D_1 t_1}{\pi}} \tag{8}$$

where t_1 is the duration of the first process, t_2 is the duration of the second process, D_2 is the diffusivity in the second stage, N is the surface density of the impurity atoms in the first stage.

The depth of the p-n junction was determined from the following equation:

$$x_j = 2\sqrt{D_2 t_2}\sqrt{\ln\left(\frac{C_{02}}{C_B}\right)}, \tag{9}$$

where C_{02} is the surface impurity concentration in the second stage $C_{02} = \frac{N}{\sqrt{\pi D_2 t_2}}$, C_B is the concentration of impurities in the original semiconductor wafer. The obtained value of p-n junction depth is $x_j = 13.4$ nm.

The effective doping concentration of n$^+$-layer was determined according to equation:

$$C_{ef} = \frac{1}{x_j}\int_0^{x_j} xC(x)dx. \tag{10}$$

It is equal to $C_{ef} = 6.15 \times 10^{19}$ cm^{-3}.

Comparison of resistances of p-region and n$^+$-region of Si NW shows the significantly (some order) higher resistance of p-region. The further reduction of series resistance of Si NW requires the optimization (increasing) diameter to length ratio of NWs.

5. Conclusions

The theoretical modeling and experimental investigations of Si NWs SC allowed to determine their optical and photoelectrical properties. The simulation of reflection, absorption and transmission of light in Si-NWs' arrays depending on their parameters, namely: diameter, length and period allowed to demonstrate the main optical properties of Si-NWs. There was a strong influence of nanowire diameter and period on light reflectance. But the effect of length was not remarkable in the investigated range. It has been found that, in comparison to Si films, the nanowire array has decreased reflection in all spectral range. In region of a long wavelength, the extinction coefficient of silicon is small and interference effects exist resulting in oscillation of reflectance and transmittance. At experimental investigations the Si-NWs arrays were formed by metal-assisted chemical etching of Si with Ag nanoparticles as a catalyst. It included a deposition of Ag nanoparticles on Si substrate from $AgNO_3$/HF solution and subsequent etching in HF/H_2O_2 resulted in the formation of 2-μm-long vertically aligned Si nanowires with diameters ranging from 60 to 160 nm. The experimental results are in agreement with theoretical ones and demonstrate lower than 1% reflectance in a wide spectral range.

The Si NWs SCs with radial p-n junction have been manufactured and their properties investigated. They showed such good parameters as $J_{sc} = 22\ mA/cm^2$, $V_{oc} = 0.62\ V$, $FF = 0.51$ and energy conversation efficiency of 7%. The analysis of dark I–V characteristics in semi-logarithmical scale revealed significant influence of shunt and series resistances.

Authorship statement

All persons who meet authorship criteria are listed as authors, and all authors certify that they have participated sufficiently in the work to take public responsibility for the content, including participation in the concept, design, analysis, writing, or revision of the manuscript. Furthermore, each author certifies that this material or similar material has not been and will not be submitted to or published in any other publication before its appearance in Opto-Electronics Review.

Acknowledgements

This work was supported in part by the National Academy of Science of Ukraine (Project No. III-10-18) and State Fund for Fundamental Research (Project No. F64/6-2016).

References

[1] X. Li, Metal assisted chemical etching for high aspect ratio nanostructures: a review of characteristics and applications in photovoltaics, Curr. Opin. Solid State Mater. Sci. 16 (2) (2012) 71–81, http://dx.doi.org/10.1016/j.cossms.2011.11.002.
[2] K.Q. Peng, S.T. Lee, Silicon nanowires for photovoltaic solar energy conversion, Adv. Mater. 23 (2011) 198–215, http://dx.doi.org/10.1002/adma.201002410.
[3] F. Es, G. Baytemir, M. Kulakci, R. Turan, Metal-assisted nano-textured solar cells with SiO_2/Si_3N_4 passivation, Solar Energy Mater. Solar Cells 160 (2017) 269–274.
[4] C.I. Yeo, Y.M. Song, S.J. Jang, Y.T. Lee, Wafer-scale broadband antireflective silicon fabricated by metal-assisted chemical etching using spin-coating Ag ink, Opt. Express 19 (2011) A1109–A1116, http://dx.doi.org/10.1364/OE.19.0A1109.
[5] C.I. Yeo, J.B. Kim, Y.M. Song, Y.T. Lee, Antireflective silicon nanostructures with hydrophobisity by metal-assisted chemical etching for solar cell application, Nanoscale Res. Lett. 8 (2013) 159, http://dx.doi.org/10.1186/1556-276X-8-159.
[6] S.K. Srivastava, D. Kumar, P.K. Singh, M. Kar, V. Kumar, M. Husain, Excellent antireflection properties of vertical silicon nanowire arrays, Solar Energy Mater. Solar Cells 94 (2010) 1506–1511, http://dx.doi.org/10.1016/j.solmat.2010.02.033.
[7] J.Y. Jung, Z. Guo, S.W. Jee, H.D. Um, K.T. Park, J.H. Lee, A strong antireflective solar cell prepared by tapering silicon nanowires, Opt. Express 8 (2010) A286–A292, http://dx.doi.org/10.1364/OE.18.00A286.
[8] S.K. Srivastava, D. Kumar, S.M. Vandana, R. Kumar, P.K. Singh, Silver catalyzed nanotexturing of silicon surfaces for solar cell applications, Solar Energy Mater. Solar Cells 100 (2012) 33–38, http://dx.doi.org/10.1016/j.solmat.2011.05.003.
[9] Y.J. Hung, S.L. Lee, L.A. Coldren, Deep and tapered silicon photonic crystals for achieving antireflection and enhanced absorption, Opt. Express 18 (7) (2010) 6841–6852, http://dx.doi.org/10.1364/OE.18.006841.
[10] S. Sharma, K.K. Jain, A. Sharma, Solar cells: in research and applications—a review, Mater. Sci. Appl. Chem. 6 (2015) 1145–1155, http://dx.doi.org/10.4236/msa.2015.612113.
[11] C. Chen, R. Jia, H. Yue, H. Li, X. Liu, D. Wu, W. Ding, T. Ye, S. Kasai, H. Tamotsu, J. Chu, S. Wang, Silicon nanowire-array-textured solar cells for photovoltaic application, J. Appl. Phys. 108 (9) (2010), http://dx.doi.org/10.1063/1.3493733, 094318–5.
[12] D. Kumar, S.K. Srivastava, P.K. Singh, M. Husain, V. Kumar, Fabrication of silicon nanowire arrays based solar cell with improved performance, Solar Energy Mater. Solar Cells 95 (1) (2011) 215–218, http://dx.doi.org/10.1016/j.solmat.2010.04.024.
[13] S. Nichkalo, A. Druzhinin, A. Evtukh, O. Bratus', O. Steblova, Silicon nanostructures produced by modified MacEtch method for antireflective Si surface, Nanoscale Res. Lett. 12 (2017) 106, http://dx.doi.org/10.1186/s11671-017-1886-2.
[14] C. Chartier, S. Bastide, C. Levy-Clement, Metal-assisted chemical etching of silicon in HF–H_2O_2, Electrochim. Acta 53 (2018) 5509–5516, http://dx.doi.org/10.1016/j.electacta.2008.03.009.
[15] D. Sullivan, J. Liu, M. Kuzyk, Three-dimensional optical pulse simulation using the FDTD method, IEEE Trans. Microw. Theory Tech. 48 (7) (2012) 1127–1133, http://dx.doi.org/10.1109/22.848495.
[16] A. Taflove, S.C. Hagness, Computational Electrodynamics: The Finite-Difference Timedomain Method, 2nd ed., Artech House, Boston, 2000.
[17] W. Sun, Q. Fu, Z. Chen, Finite-difference time-domain solution of light scattering by dielectric particles with a perfectly matched layer absorbing boundary condition, Appl. Opt. 38 (15) (1999) 3141–3151, http://dx.doi.org/10.1364/AO.38.003141.
[18] A. Deinega, I. Valuev, Long-time behavior of PML absorbing boundaries for layered periodic structures, Comput. Phys. Commun. 182 (1) (2011) 149–151, http://dx.doi.org/10.1016/j.cpc.2010.06.006.
[19] J. Li, H. Yu. Yu, Sh. M. Wong, X. Li, G. Zhang, Patrick Guo-Qiang Lo, Dim-Lee Kwong, Design guidelines of periodic Si nanowire arrays for solar cell application, Appl. Phys. Lett. 95 (2009) 243113, http://dx.doi.org/10.1063/1.3275798.
[20] P. Gao, H. Wang, Z. Sun, W. Han, J. Li, J. Ye, Efficient light trapping in low aspect-ratio honeycomb nanobowl surface texturing for crystalline silicon solar cell applications, Appl. Phys. Lett. 103 (2013) 253105, http://dx.doi.org/10.1063/1.4851236.
[21] F. Wang, J. Li, H.Yu. Yu, Optimization of periodic nanopore surface texturing for silicon thin film photovoltaic application, 3rd International Nanoelectronics Conference (INEC) (2010), http://dx.doi.org/10.1109/INEC.2010.5424863.
[22] O.V. Pylypova, A.A. Evtukh, P.V. Parfenyuk, I.M. Korobchuk, O.O. Havryliuk, O.Yu. Semchuk, Influence of Si nanowires on solar cell properties: effect of the temperature, Appl. Phys. A 124 (2018) 773, http://dx.doi.org/10.1007/s00339-018-2200-6.
[23] M.L. Zhang, X.Q. Peng, X. Fan, J.S. Jie, R.Q. Zhang, S.T. Lee, N.B. Wong, Preparation of large-area uniform silicon nanowires arrays through metal-assisted chemical etching, J. Phys. Chem. C 112 (12) (2008) 4444–4450, http://dx.doi.org/10.1021/jp077053o.
[24] X. Li, P.W. Bohn, Metal-assisted chemical etching in HF/H2O2 produces porous silicon, Appl. Phys. Lett. 77 (2000) 2572, http://dx.doi.org/10.1063/1.1319191.
[25] K.Q. Peng, S.T. Lee, Silicon nanowires for photovoltaic solar energy conversion, Adv. Mater. 23 (2011) 198, http://dx.doi.org/10.1002/adma.201002410.
[26] M.A. Green, M.J. Keevers, Optical properties of intrinsic silicon at 300 K, Prog. Photovolt. Res. Appl. 3 (3) (1995) 189–192, http://dx.doi.org/10.1002/pip.4670030303.
[27] J. Li, H.Yu. Yu, S.M. Wong, G. Zhang, X. Sun, P.G.Q. Lo, D.L. Kwong, Si nanopillar array optimization on Si thin films for solar energy harvesting, Appl. Phys. Lett. 95 (2009) 033102, http://dx.doi.org/10.1063/1.3186046.
[28] J. Li, S.M. Wong, Y. Li, H. Yu. Yu, High-efficiency crystalline Si thin film solar cells with Si nanopillar array textured surfaces, 35th IEEE Photovoltaic Specialists Conference (2010), http://dx.doi.org/10.1109/PVSC.2010.5614445.
[29] J. Li, H.Yu. Yu, Y. Li, F. Wang, M. Yang, S.M. Wong, Low aspect-ratio hemispherical nanopit surface texturing for enhancing light absorption in crystalline Si thin film-based solar cells, Appl. Phys. Lett. 98 (2011) 021905, http://dx.doi.org/10.1063/1.3537810.
[30] L.P. Avakyants, P.Yu. Bokov, A.V. Chervyakov, A.V. Chuyas, A.E. Yunovich, E.D. Vasileva, D.A. Bauman, V.V. Uelin, B.S. Yavich, Interference effects in the electroreflectance and electroluminescence spectra of InGaN/AlGaN/GaN light-emitting-diode heterostructures, Semiconductors 44 (2010) 1090, http://dx.doi.org/10.1134/S1063782610080245.
[31] B.C.P. Sturmberg, K.B. Dossou, L.C. Botten, A.A. Asatryan, C.G. Poulton, C.M. Sterke, R.C. McPhedran, Modal analysis of enhanced absorption in silicon nanowire arrays, Opt. Express 19 (S5) (2011) A1067, http://dx.doi.org/10.1364/OE.19.0A1067.
[32] S.M. Sze, Semiconductors Devices Physics and Technology, 2nd edition, John Wiley & Sons, Inc., USA, 2002.